RSC Advances

PAPER

View Article Online
View Journal | View Issue

Cite this: *RSC Adv.*, 2017, **7**, 45432

Theoretical insights into the structural, relative stable, electronic, and gas sensing properties of Pb_nAu_n (n = 2–12) clusters: a DFT study†

Gaofeng Li,[bc] Xiumin Chen,[*abc] Zhiqiang Zhou,[abc] Fei Wang,[bc] Hongwei Yang,[bc] Jia Yang,[bc] Baoqiang Xu,[bc] Bin Yang[bc] and Dachun Liu[bc]

Recently, Au-based clusters have been provoking great interest due to their potential applications in nanotechnology. Herein, the structural, relative stable, electronic, and gas sensing properties of Pb_nAu_n (n = 2–12) clusters were systematically investigated using density functional theory together with scalar relativistic pseudopotential. The ground state structures, average binding energies, dissociation energies, second order energy differences, HOMO–LUMO gaps, and average Mulliken charges of Pb_nAu_n (n = 2–12) clusters were calculated. The results revealing that the Pb_nAu_n (n = 4, 6, and 8) clusters are more relatively stable than their neighboring clusters. Furthermore, charges are always transferred from the Pb atoms to Au atoms based on Mulliken charge analysis. Furthermore, through the investigations of CO or NO molecule adsorption onto Pb_nAu_n (n = 4, 6, and 8) clusters, it is found that CO or NO molecule can chemisorb on those clusters with high sensitivity, and the charges are transferred from Pb_nAu_n (n = 4, 6, and 8) clusters to the gas molecules. According to the analysis of the electric conductivity, Pb_nAu_n (n = 4, 6, and 8) clusters can be served as potential gas sensors in CO and NO molecules detection.

Received 22nd August 2017
Accepted 17th September 2017

DOI: 10.1039/c7ra09286e

rsc.li/rsc-advances

1. Introduction

In recent years, clusters have drawn considerable attention from all over the world. The mesoscopic or macroscopic properties of clusters can be investigated at an atomic or molecular level,[1–3] which are governed by geometrical structure, cluster size and chemical composition.[2,4–7] In particular, Au_n clusters and Au-based clusters have been extensively studied using theoretical calculations and experimental investigations since they have been found to serve as potential applications in nanostructured materials,[8] electronic devices,[9] optical limiting materials,[10] sensor technologies,[9,11] and nano-catalytic systems,[12–15] *etc.*

The investigations of Au_n clusters are important to the deep investigations of Au-based clusters, because the fundamental investigations of Au_n clusters may provide some valuable guidance for that of Au-based clusters. Overall, pure Au_n clusters have been more systematically investigated than Au-based clusters. It is well known that the properties of Au_n clusters are very sensitive to both size n and geometrical structure. According to the theoretical calculations,[16–22] the ground-state structures of Au_n clusters demonstrate a transition from two-dimensional structures to three-dimensional structures due to the strong relativistic effects in Au atoms.[23,24] In general, Au_n (n = 3–13) clusters favor planar structures, whereas those Au_n clusters exhibit three-dimensional structures when the size n is larger than 13. In order to uncover the structural, energetic and electronic properties of Au_n (n = 3–14) clusters, Li *et al.*[19] carried out systematical calculations by density functional theory, the results show that those Au_n clusters with even numbers of atoms are more stable than their neighboring clusters, and the two-dimensional to three-dimensional transition occurs at n = 12. De Bas *et al.*[25] employed a combination of empirical potentials and first principles method to further explore the low energy structures of the large Au_n (n = 3–38) nanoclusters. It is found that the Au_n clusters are disordered and could be stable at room temperature. However, the promising applications of Au_n clusters are also particularly interesting to scholars. For example, Gautam *et al.*[18] systematically investigated the C_2H_2 activation and hydrogenation of C_2H_2 activated on small Au_n (n = 3–10) clusters using DFT calculations. Zhou *et al.*[26] performed ultrafast spectroscopic investigations on atomically precise thiolate-protected Au_n nanoparticles, the Au_n nanoparticles show three distinct states, including metallic, transition regime and non-metallic or excitonic states and their catalytic properties were obviously changed.

Nowadays, bimetallic clusters have drawn more considerable attention than monatomic clusters. Bimetallic clusters exhibit more intriguing properties than both pure clusters due to the

[a]State Key Laboratory of Complex Nonferrous Metal Resources Clear Utilization, Kunming University of Science and Technology, Kunming 650093, PR China. E-mail: chenxiumin9@hotmail.com

[b]National Engineering Laboratory for Vacuum Metallurgy, Kunming University of Science and Technology, Kunming 650093, PR China

[c]Yunnan Provincial Key Laboratory for Nonferrous Vacuum Metallurgy, Kunming University of Science and Technology, Kunming 650093, PR China

† Electronic supplementary information (ESI) available. See DOI: 10.1039/c7ra09286e

synergetic effects between the two different atoms in bimetallic clusters,[13] which provide a new technological and fundamental point of view as well as wide range of applications in nanotechnology. First of all, fundamental investigations of bimetallic clusters are crucial to the further applications. There are many evidences. For the sake of discovering electronic and magnetic properties of MAu_6^- (M = Ti, V, Cr) clusters, Li *et al.*[27] applied a combination of density functional theory and photoelectron spectroscopy (PES) scheme, with the results indicating that all the anionic and neutral clusters possess planar structures and large magnetic moments, in which the doped transition atom lies in the center of the Au_6 ring. Wen *et al.*[28,29] investigated the structures of $Au_xS^{0,\pm1}$ (x = 2–10) clusters by means of theoretical calculations and experimental study, it is found that the transition of 1D-to-2D-to-3D was observed owing to the strong S–Au covalent bond, delocalized Au–Au bond, strong relativistic effects of Au and electronegativity between Au and S. The 3D assignment of structures of Au_8M (M = Si, Ge, Sn) anion clusters were investigated by Liu *et al.*,[30] it is found that the ground state structures of anion Au_8Ge cluster and anion Au_8Sn cluster are different from the results in previous studies. Furthermore, the promising applications of bimetallic Au-based clusters have been receiving great interest ever before. Mondal *et al.*[12] investigated the structure and chemical reactivity of $Au_{19}Pt$ binary cluster within density functional theory, the results show that the tetrahedral structures of $Au_{19}Pt$ clusters are particularly stable, and CO molecule adsorption on the bare Pt site are favorable in tetrahedral $Au_{19}Pt$ clusters. Kauffman *et al.*[31] investigated $Au_{25-x}Ag_x$ binary cluster by computational and experimental characterization, the results demonstrate that the Ag atom preferentially occupy the surface of the cluster, resulting $Au_{25-x}Ag_x$ cluster as a candidate in photo-mediated charge-transfer event. Yong *et al.*[11] theoretically investigated the potential applications of Ag_7Au_6 cluster in gas sensing, it is found that the Ag_7Au_6 cluster show good chemisorbing characteristic of CO, HCN and NO molecules, which may has a promising gas sensor applications in CO, HCN and NO gases detection.

To the best of our knowledge, no systematical work has been reported on the Pb_nAu_n clusters. In this work, the structural, relative stable, electronic, and gas sensing properties of Pb_nAu_n (n = 2–12) clusters were systematically studied by density functional theory to explore the fundamental characters and promising applications of Pb_nAu_n (n = 2–12) clusters. It is well known that bimetallic Au-based novel clusters may have great novel properties, and the development of the functional nanomaterials based on earth-abundant and alternative cheap metal elements to replace the novel elements for functionally Au-based cluster catalysis are promising. Additionally, the toxic CO and NO gas molecules have become an increasing urgent environment problem owing to mainly combustion of fossil fuel, which have been posing great threats to humans' health. Hence, the toxic gases monitoring are extremely important with regard to the serious environment at present. Therefore, we firmly believe that this systematically theoretical investigation of Pb_nAu_n (n = 2–12) clusters would help us to uncover the fundamental characteristic of these clusters and their promising applications in gas detection.

2. Computational details

In the present work, all the calculations were carried out using spin-polarized density functional theory (DFT) as implemented in the DMol^3 package.[11,32,33] Initially, the GGA-PW91 functional,[11,34] GGA-PBE functional,[12,35] and GGA-BLYP[36] functional were employed to treat the exchange and correlation energy for Pb_2 dimer, Au_2 dimer and PbAu cluster. The results demonstrate that the GGA-PW91 functional yields the parameters of the dimers which are closer to the experimental data, as shown in Table S1 (ESI†). Therefore, the GGA-PW91 functional was chosen in all the following calculations. All electron relativistic pseudopotentials were employed to treat the strong relativistic effects for Pb_nAu_n clusters due to the energetically close between the destabilization of the $5d^{10}$ orbitals and stabilization of the $6s^1$ orbit in Au atom.[23,32] The double-numerical basis set plus d polarization functions (DNP)[33] was chosen in this work. The extensive isomers were generated using *ab initio* molecular dynamics in which time step is 1 fs, total simulation time is 100 ps, temperature is 300 K, ensemble is NVT[37] with constant temperature and constant volume. Possible spin multiplicities (singlet, triplet, quintet and septet were used to treat those Pb_nAu_n clusters with closed-shell electronics, whereas double, quartet, sextet and octet were chosen to treat those Pb_nAu_n clusters with open-shell electronics) were also taken into account during the geometry optimization processes because the polarization may have potential effects on the structures of Pb_nAu_n clusters. It is interesting to point out that all optimized geometries were found to adopt the corresponding lowest spin states. The same results during the geometry optimization processes of the bimetallic M_2-doped Au_n (M = Cu, Ag; n = 1–10) clusters were also found by Zhao *et al.*[8] The SCF threshed is 10^{-6} Ha on the total energy. Convergence tolerance: 10^{-5} Ha, 0.002 Ha Å^{-1} and 0.005 Å are for energy, maximum force and maximum displacement, respectively. The smearing (0.005 Ha) was used to achieve good convergence results. Harmonic vibration frequencies were calculated to verify no imaginary frequency in the ground-state structures of Pb_nAu_n clusters. It is indispensable to mention that the density of states (DOS) were calculated using DFT Semi-core Pseudopotentials (DSPPs) with fitting all-electron relativistic DFT calculations. We are confident that the calculation methods in this work are reliable and accurate enough for investigating the Pb_nAu_n (n = 2–12) clusters, because our calculated results are in excellent agreement with the experimental data, as shown in Table S1 (ESI†).

3. Results and discussion

3.1. The ground-state structures and growth pattern of Pb_nAu_n (n = 2–12) clusters

We initially built the structure of Pb_nAu_n cluster which was optimized using geometry optimization calculations. Then the optimized structure was served as the initial structure of *ab initio* molecular dynamics calculations. The isomers of Pb_nAu_n

clusters were generated using *ab initio* molecular dynamics calculations, then the obtained low-lying isomers were optimized, and then the ground state structures of Pb_nAu_n clusters were achieved by comparing the energies of the optimized low-lying isomers. Fig. 1 shows the lowest energy structures of the Pb_nAu_n (n = 2–14) clusters after the *ab initio* molecular dynamics simulations and geometry optimizations of local minimum isomers of Pb_nAu_n clusters, whereas the second lowest energy structures are shown in Fig. S1 (ESI†). As we can see from the Fig. 1, the Pb_2Au_2 cluster is a triangular pyramid with C_{2V} symmetry, which yields a huge difference to the Pb_4 cluster and Au_4 cluster since the Pb_4 cluster and the Au_4 cluster prefer planar geometries.[19,38] The Pb_3Au_3 cluster is a rectangular pyramid which is capped by an additional Au atom, and shows no symmetry. For the Pb_4Au_4 cluster, its geometrical structure seems to be complicated, exhibiting C_s symmetry, and the Au atoms evenly distributed on the surface of the cluster. The Pb_5Au_5 cluster is composed of two parts which are a distorted quadrangular and a triangular prism, and shows no symmetry. The ground state structure of the Pb_6Au_6 cluster is the 3D configuration without any symmetry, in which the six gold atoms bond together and occupy on the side of the cluster. The most stable structure of the Pb_7Au_7 cluster is distorted with no symmetry, and only six gold atoms bond together but the rest of the Au atoms is separated by two Pb atoms. From n = 8 to n = 12, we clearly see that those Pb_nAu_n clusters show a difference to those Pb_nAu_n (n = 2–7) clusters, which gold atoms aggregate together and occupy the central sites of the clusters. Moreover, all the Pb_nAu_n (n = 8–12) clusters are no symmetry except for the Pb_8Au_8 cluster is the 3D configuration with C_s symmetry. The aggregation effects of gold atoms in the central sites of Pb_nAu_n clusters are originated from the atomic radius of Au atom (1.44 Å) is smaller than that of Pb atom (1.75 Å). The similar phenomenon was also found by other researchers.[39–41] It is interesting to note that the Pb_nAu_n (n = 2–12) clusters don't exhibit distinct rule of symmetry due to the equal ratio of Pb atoms and Au atoms for Pb_nAu_n clusters and the Jahn–Teller effects. Additionally, the cluster with a lower symmetry can decrease its total energy to some extent based on the Jahn–Teller theory.[42] Particularly, it is concluded that Au atoms have strong interactions with the Pb atoms, because the Pb_n clusters and Au_n clusters are in favor of planar structures when the cluster size n is small while the Pb_nAu_n (n = 2–12) clusters are in favor of three dimensional structures.[16,18,38,43]

3.2. Average binding energies and stabilities of Pb_nAu_n (n = 2–12) clusters

In order to predict the relative stabilities of the ground state structures of Pb_nAu_n (n = 2–12) clusters, the average binding energies (E_b), the fragmentation energies (ΔE), and the second order energy differences ($\Delta_2 E$) of Pb_nAu_n (n = 2–12) clusters are calculated. For Pb_nAu_n clusters, the E_b, ΔE, and $\Delta_2 E$ are defined using the following formulas[36,44,45]

$$E_b(Pb_nAu_n) = [nE(Pb) + nE(Au) - E(Pb_nAu_n)]/2n$$

$$\Delta E(Pb_nAu_n) = E(Pb_{n-1}Au_{n-1}) + E(PbAu) - E(Pb_nAu_n)$$

$$\Delta_2 E(Pb_nAu_n) = E(Pb_{n-1}Au_{n-1}) + E(Pb_{n+1}Au_{n+1}) - 2E(Pb_nAu_n)$$

where E(Pb), E(Au), $E(Pb_{n-1}Au_{n-1})$, $E(Pb_nAu_n)$, and $E(Pb_{n+1}Au_{n+1})$ represent the total energies of the Pb atom, Au atom,

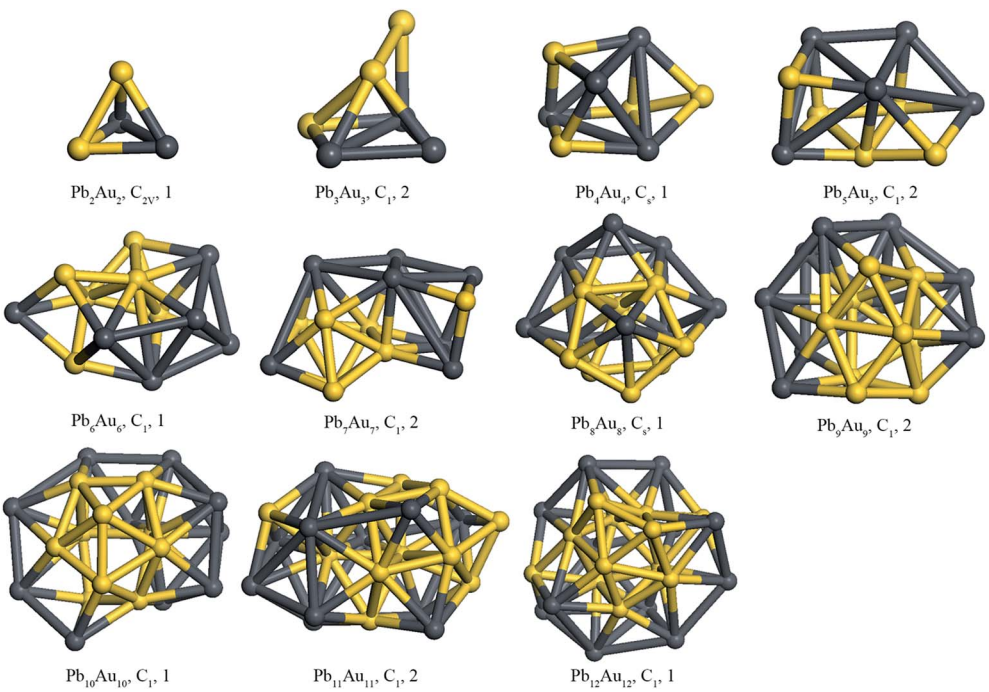

Fig. 1 Lowest energy structures of Pb_nAu_n (n = 2–12) clusters. Spin multiplicity states and the corresponding point group symmetries of Pb_nAu_n (n = 2–12) clusters are also given, which follow the corresponding Pb_nAu_n clusters. The dark grey ball is Pb atom, and yellow ball is Au atom.

$Pb_{n-1}Au_{n-1}$ cluster, Pb_nAu_n cluster, and $Pb_{n+1}Au_{n+1}$ cluster, respectively. The calculated E_b, ΔE, and $\Delta_2 E$ values of the ground state structures of Pb_nAu_n (n = 2–12) clusters as the functions of cluster size n are shown in Fig. 2. The average binding energy is a good index to denote the thermodynamics stabilities of the clusters. As can be seen from the Fig. 2, the average binding energies increase with the increasing cluster size n, and approach to be stable when cluster size $n \geq 10$, indicating that ground state structures of Pb_nAu_n clusters tend to be stable when cluster size $n \geq 10$. Overall, the curve of average binding energies against the corresponding cluster size n can be divided into four parts based on the slopes between those parts. The first part is in the range of n = 2–3, the second part is in the range of n = 4–7, the third part is in the range of n = 8–9, and the last part is the range of n = 10–12. Furthermore, it is interesting to point out that the slopes between those parts show a big difference to both of the adjacent parts. A sharply decrease of the slope of the first part, which may be originated from the geometrical compactness of the Pb_3Au_3 cluster is much larger than that of Pb_2Au_2 cluster. It is indicated that the slope of the second part shows relative slow increase but the slop between the first part and the second part is large, which means the geometrical structures of the Pb_nAu_n clusters within the second part doesn't exhibit an essential difference to each other, whereas the geometrical structures of the Pb_nAu_n clusters within the second part shows a huge difference to that of the first part. Similarly, the geometrical structures of the third part reveal a very small difference within the interval, but showing a huge difference to the second part. The average binding energies tend to be stable in the last part, which indicates the geometrical structures of Pb_nAu_n (n = 10–12) clusters are stable.

In order to further study the stabilities of the ground state structures of Pb_nAu_n clusters, we will also discuss the fragmentation energies and second order energy differences of Pb_nAu_n (n = 2–12) clusters. From the given formulas mentioned above, a higher value of fragmentation energy corresponding to a higher stability of the cluster due to more energy is needed if the Pb_nAu_n cluster dissociates into a smaller PbAu cluster and a smaller $Pb_{n-1}Au_{n-1}$ cluster. Moreover, the definition of second order energy difference is similar to that of fragmentation energy, the second order energy differences can reflect the relative stabilities of neutral clusters compared to their neighbors. It is suggested that the cluster is more stable with a higher value of second order energy difference. As shown in Fig. 2, the size dependence of the fragmentation energies and second order energy differences show obvious odd–even alternation phenomena, and the general trends are in good agreement with each other. Therefore, it is interesting to find that the cluster with even number of electrons is more stable than their neighbors with odd number of electrons. In addition, four obvious peaks are observed at n = 4, 6, 8, and 10, revealing that the Pb_4Au_4 cluster, Pb_6Au_6 cluster, Pb_8Au_8 cluster, and $Pb_{10}Au_{10}$ cluster are more stable than their neighbors.

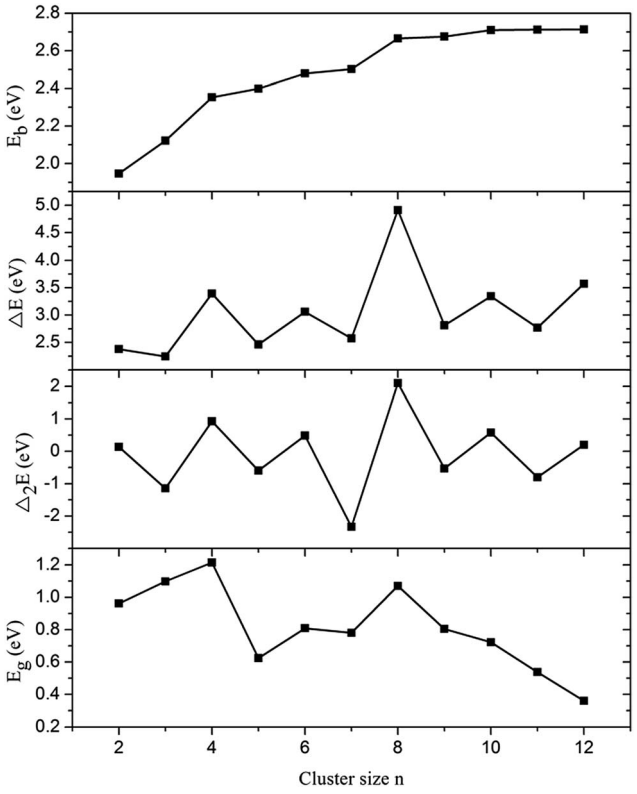

Fig. 2 Average binding energies (E_b), fragmentation energies (ΔE), and second order energy differences ($\Delta_2 E$) of Pb_nAu_n (n = 2–12) clusters *versus* the cluster size n.

3.3. HOMO–LUMO gaps and Mulliken charge analysis

The HOMO–LUMO gap (E_g) is of great interest due to its reflection of the kinetic stability, chemical stability, and electrical conductivity of the cluster.[46,47] HOMO–LUMO gap demonstrates the energy gap between the highest occupied orbit and the lowest unoccupied orbit for a cluster. A higher value of HOMO–LUMO gap corresponds to a high energy required for electrons jump from the occupied orbit to unoccupied orbit. In a word, a smaller value of HOMO–LUMO gap represents a higher chemical reactivity, whereas a higher value of HOMO–LUMO gap indicates a weaker chemical reactivity. HOMO–LUMO gaps of Pb_nAu_n (n = 2–12) clusters are listed in Table 1, and the relationship between the HOMO–LUMO gaps and the corresponding cluster size n are shown in Fig. 2. As presented in the Fig. 2, it is seen that the HOMO–LUMO gaps show a general decreasing tendency with the increasing cluster size n, which means the chemical reactivity of the Pb_nAu_n clusters decrease with the increasing cluster size n. In addition, the Pb_4Au_4 cluster, Pb_6Au_6 cluster and Pb_8Au_8 cluster are found with relatively higher values of HOMO–LUMO gaps than their neighbouring clusters. Therefore, we draw a conclusion that the Pb_nAu_n (n = 4, 6, and 8) clusters have relatively stable chemical reactivity. It is in well agreement with the analysis of fragmentation energies and second-order energy in differences mentioned above. To further analyse the electronic structures of the Pb_4Au_4 cluster, Pb_6Au_6 cluster, and Pb_8Au_8 cluster, it is important to find that valence electrons of the Pb_4Au_4 cluster, Pb_6Au_6 cluster, and Pb_8Au_8 cluster are 20 electrons, 30 electrons and 40 electrons, respectively. The electron configurations of

Table 1 HOMO–LUMO gaps and average Mulliken charges (positive value represents the donation of electrons while negative value represents the acceptance of electrons) of Pb_nAu_n (n = 2–12) clusters

PbnAun cluster	HOMO–LUMO gap (eV)	Average Mulliken charge (e)	
		Pb atoms	Au atoms
$n = 2$	0.961	0.272	−0.272
$n = 3$	1.098	0.247	−0.247
$n = 4$	1.214	0.291	−0.291
$n = 5$	0.624	0.261	−0.261
$n = 6$	0.808	0.228	−0.228
$n = 7$	0.780	0.235	−0.235
$n = 8$	1.070	0.232	−0.232
$n = 9$	0.804	0.189	−0.189
$n = 10$	0.722	0.200	−0.200
$n = 11$	0.538	0.254	−0.254
$n = 12$	0.360	0.223	−0.223

the Pb_nAu_n (n = 4, 6, and 8) clusters are in excellent agreement with the Jellium model that the cluster with distinct close-shell electronics is particularly chemical stable.[48,49] We can further conclude that the chemical stabilities of the Pb_4Au_4 cluster, Pb_6Au_6 cluster, and Pb_8Au_8 cluster are enhanced. Therefore, the Pb_4Au_4 cluster, Pb_6Au_6 cluster, and Pb_8Au_8 cluster may be the stable building blocks, and can be used in novel nanomaterials. The potential adsorption properties of the stable clusters will be further investigated in this work.

To unravel the reliable charge transfer information of Pb_nAu_n (n = 2–12) clusters, the average Mulliken charges were calculated, the results are given in Table 1. The values of average Mulliken charges for Pb atoms in Pb_nAu_n clusters are positive and that of for Au atoms in Pb_nAu_n clusters are negative, indicating that the charges always transfer from Pb atoms to Au atoms in Pb_nAu_n clusters since the electronegativity of Au (2.54 for Au, according to Pauling) is larger than that of that Pb (2.33 for Pb, according to Pauling). This interesting phenomenon is in excellent agreement with our previous work about Pb_nCu_n clusters[36] and other scholars' results.[8,47,50] Therefore, we can conclude that the Pb atoms act as the electron donors while Au atoms act as the electron acceptors in Pb_nAu_n clusters. The electron accumulation of Au atoms in Pb_nAu_n clusters may be the most active sites during the catalytic and adsorption processes.

3.4. Gas adsorption properties of the Pb_4Au_4 cluster, Pb_6Au_6 cluster and Pb_8Au_8 cluster

According the detailed discussions on Pb_nAu_n (n = 2–12) clusters mentioned above, the Pb_4Au_4 cluster, Pb_6Au_6 cluster and Pb_8Au_8 cluster are relatively more stable than other Pb_nAu_n clusters, and may serve as the building blocks for the design of cluster-assemble nanomaterials due to their chemically stable reactivity. Then, we will investigate the feasibility of CO or NO molecule adsorption on the ground-state structures of the three clusters with tailored properties. For Pb_nAu_n–CO (n = 4, 6, and 8) and Pb_nAu_n–NO (n = 4, 6, and 8) complexes, the adsorption energy (E_{ads}) of CO molecule (or NO) molecule on Pb_nAu_n clusters can be defined as follows[11,18]

$$E_{ads} = E(Pb_nAu_n\text{–CO}) - E(Pb_nAu_n) - E(CO)$$

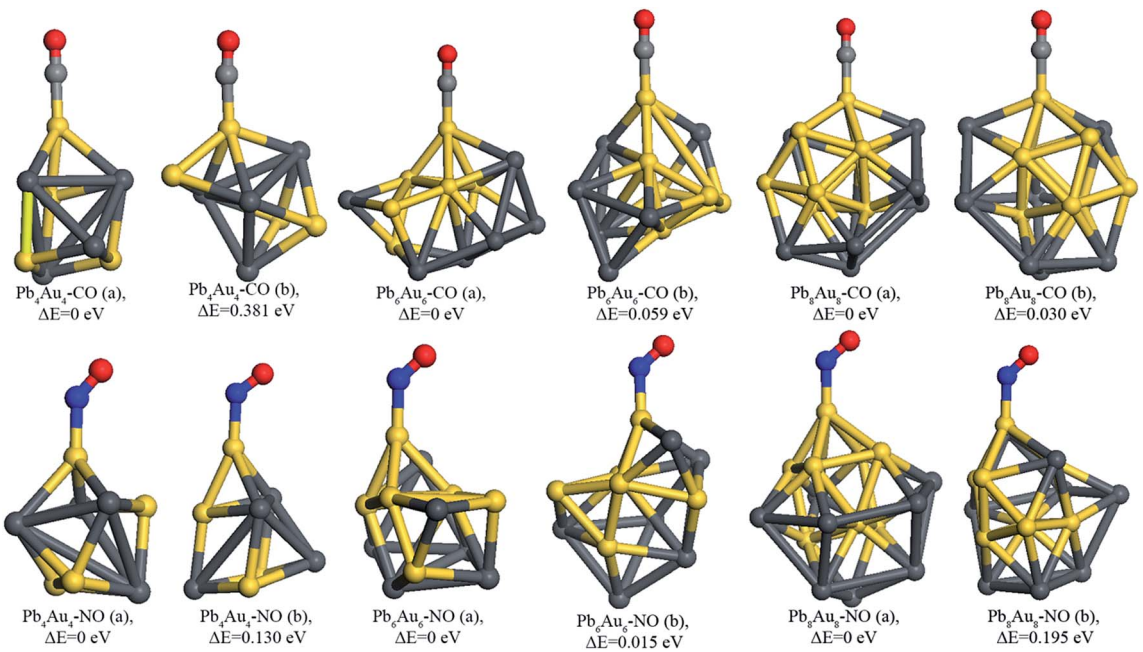

Fig. 3 The stable configurations of Pb_nAu_n–CO and Pb_nAu_n–NO (n = 4, 6, and 8) complexes. The configuration a represents the most stable configuration while configuration b stands for the second stable configuration of the corresponding Pb_nAu_n–CO (n = 4, 6, and 8) complexes and Pb_nAu_n–NO (n = 4, 6, and 8) complexes. The dark gray ball is Pb atom, yellow ball is Au atom, grayish ball is C atom, red ball is O atom, and blue ball is N atom.

$$E_{ads} = E(Pb_nAu_n\text{–NO}) - E(Pb_nAu_n) - E(NO)$$

where $E(Pb_nAu_n\text{–CO})$, $E(Pb_nAu_n\text{–NO})$, $E(Pb_nAu_n)$, $E(CO)$, and $E(NO)$ are the energies of Pb_nAu_n–CO, Pb_nAu_n–NO, Pb_nAu_n, CO, and NO species, respectively. According to the formula of the definition of adsorption energy, the molecule is easy to bind to Pb_nAu_n cluster and it is a exothermal reaction when $E_{ads} < 0$, whereas it impossible for a molecule bind to the Pb_nAu_n cluster when $E_{ads} > 0$.

In this work, every possible adsorption sites (all the bare Pb atoms and Au atoms) were taken into consideration. Moreover, the orientation of C atom pointing to adsorption site and that of O atom pointing to adsorption site for CO molecule adsorption on Pb_nAu_n (n = 4, 6, and 8) clusters were also taken into consideration. After full geometry relaxation of all possible initial configurations, C or N atom directly binds to Au atoms of Pb_nAu_n (n = 4, 6, and 8) clusters are energetically favorable, which means Au atoms are the active sites for molecule adsorption. Interestingly, it is worthy to note that the active sites of Pb_nAu_n clusters are in well agreement with the analysis of the average Mulliken charges discussed above. The most stable and second stable configurations of CO molecule adsorption on Pb_4Au_4, Pb_6Au_6, and Pb_8Au_8 clusters are shown in Fig. 3.

According to the most stable configurations of CO molecule adsorption on Pb_nAu_n clusters (n = 4, 6, and 8), the CO molecule prefers the orientation of the C atom directly binding to the Pb_nAu_n clusters and C atom of CO molecule is located on the top of Au atom, which is consistent with the work reported by other literature.[11,51,52] Moreover, the CO molecule almost in the straight line with absorbed Au atom and the Au–C–O angles are in the range of 175.418–179.007°. The distances between the C atom and active Au atoms are in the range of 1.875–1.902 Å, as shown in Table 2, revealing that the adsorption processes are enhanced compared to the distances between C atom and Ag atom (or Au atom) of Ag_7Au_6–CO complexes are in the range of 2.099–2.002 Å.[11] It is concluded that the configurations of Pb_n-Au_n–CO (n = 4, 6, and 8) complexes do not show big differences when CO molecule adsorption on the different adsorption sites of Pb_nAu_n (n = 4, 6, and 8) clusters. The adsorption energies are in the range of −1.062–1.498 eV, as shown in Table 2, indicating that CO molecule is chemisorbed onto the Pb_nAu_n (n = 4, 6, and 8) clusters. The adsorption energies are larger than that of CO molecule adsorbed onto the Ag_7Au_6 cluster, the contributions of Pb atoms in Pb_nAu_n (n = 4, 6, and 8) clusters may be responsible for the enhanced chemical adsorption. Moreover, it is found that charges are always transferred from the Pb_nAu_n clusters to CO molecule, as shown in Table 2. The charges were calculated using Hirshfeld method due to the Hirshfeld method can obtain more reliable results than Mulliken, Bader, and Weinhold methods.[11] This trend of electron transfer is similar to the previous work reported by Yong *et al.*[11] In order to unravel the charges transfer from the Pb_nAu_n (n = 4, 6, and 8) clusters to the CO molecule, we calculated the vibrational frequencies of the –CO moieties in the Pb_nAu_n–CO (n = 4, 6, and 8) complexes, and the vibrational frequency of the isolated CO molecules in the gas phase, as shown in Table 3. From the table, we can see that the vibrational frequencies of the –CO moieties in the Pb_nAu_n–CO (n = 4, 6, and 8) complexes are decreased as compared to the vibrational frequency of the isolated CO molecule in the gas phase. Obviously, the red shifts of the vibrational frequencies of –CO moieties are achieved. It can be used to explain the charges transfer from the Pb_nAu_n clusters to CO molecule.

In order to uncover the reaction mechanisms that charges always transfer from Pb_nAu_n clusters to CO molecule when CO molecule adsorption onto Pb_nAu_n (n = 4, 6, and 8) clusters. The energy levels of HOMOs and LUMOs for CO molecule and Pb_nAu_n clusters were calculated, respectively, as listed in Table 4. The energy differences between LUMO of CO molecule and HOMOs of Pb_nAu_n (n = 4, 6, and 8) clusters are in the range of 2.564–2.645 eV, whereas that of HOMO of CO molecule and LUMOs of Pb_nAu_n (n = 4, 6, and 8) clusters are in the range of 5.411–5.636 eV. It is obvious that the energy gaps of HOMO–LUMO ($Pb_nAu_n \rightarrow$ CO) are smaller than that of HOMO–LUMO (CO $\rightarrow$ Pb_nAu_n), and HOMOs of Pb_nAu_n (n = 4, 6, and 8) clusters overlap well with LUMO of CO molecule, as shown in Fig. 4.

Table 2 The calculated adsorption energies (E_{ad}), the distances (D, viewed as the lowest distance between the adsorption site and CO) between CO and Pb_nAu_n clusters, charges transfer (Q_T) from the Pb_nAu_n clusters to CO molecule (the charges were calculated using Hirshfeld method), HOMO–LUMO gaps (E_g) for Pb_nAu_n–CO (n = 4, 6, and 8) complexes, and ΔE_g represents HOMO–LUMO gap differences between Pb_nAu_n clusters and Pb_nAu_n–CO (n = 4, 6, and 8) complexes ($\Delta E_g = E_g(Pb_nAu_n) - E_g(Pb_nAu_n\text{–CO})$)

Configuration	E_{ads} (eV)	D (Å)	Q_T (e)	E_g (eV)	ΔE_g (eV)
Pb_4Au_4–CO(a)	−1.443	1.878	0.029	0.992	0.222
Pb_4Au_4–CO(b)	−1.062	1.902	0.045	1.057	0.157
Pb_6Au_6–CO(a)	−1.498	1.875	0.044	0.546	0.262
Pb_6Au_6–CO(b)	−1.439	1.875	0.032	0.577	0.209
Pb_8Au_8–CO(a)	−1.355	1.885	0.057	0.721	0.349
Pb_8Au_8–CO(b)	−1.325	1.884	0.045	0.719	0.315

Table 3 υ_a represents the vibrational frequencies of –CO (or –NO) moieties in the corresponding lowest energy isomers of Pb_nAu_n–CO (or Pb_nAu_n–NO) complexes and υ_b represents the vibrational frequencies of –CO (or –NO) moieties in the corresponding second lowest energy isomers of Pb_nAu_n–CO (or Pb_nAu_n–NO) complexes (υ_a also represents the vibrational frequency of CO (or NO) molecule in the gas phase). $\Delta\upsilon_a$ represents the vibrational frequency differences between CO (or NO) molecule and the lowest energy isomers of Pb_nAu_n–CO (or Pb_nAu_n–NO) complexes ($\Delta\upsilon_a = \upsilon_a(CO) - \upsilon_a(Pb_nAu_n\text{–CO})$ or $\Delta\upsilon_a = \upsilon_a(NO) - \upsilon_a(Pb_nAu_n\text{–NO})$). Similarly, $\Delta\upsilon_b$ represents the vibrational frequency differences between CO (or NO) molecule and the second lowest energy isomers of Pb_nAu_n–CO (or Pb_nAu_n–NO) complexes ($\Delta\upsilon_b = \upsilon_a(CO) - \upsilon_b(Pb_nAu_n\text{–CO})$ or $\Delta\upsilon_b = \upsilon_a(NO) - \upsilon_b(Pb_nAu_n\text{–NO})$)

System	υ_a (cm^{-1})	υ_b (cm^{-1})	$\Delta\upsilon_a$ (cm^{-1})	$\Delta\upsilon_b$ (cm^{-1})
CO	2119.91			
NO	1893.46			
Pb_4Au_4–CO	2038.65	2028.11	81.26	91.8
Pb_6Au_6–CO	2054.94	2045.35	64.97	74.56
Pb_8Au_8–CO	2031.63	2069.86	88.28	50.05
Pb_4Au_4–NO	1640.74	1632.55	252.72	260.91
Pb_6Au_6–NO	1649.30	1633.92	244.16	259.54
Pb_8Au_8–NO	1652.42	1635.32	241.04	258.14

Table 4 The energy levels of HOMOs and LUMOs of CO molecule and Pb_nAu_n (n = 4, 6, and 8) clusters, and their energy gaps between CO and Pb_nAu_n (n = 4, 6, and 8) clusters (energies in eV)

System	HOMO	LUMO	HOMO–LUMO (Pb_nAu_n → CO)	HOMO–LUMO (CO → Pb_nAu_n)	HOMO–LUMO (Pb_nAu_n → NO)	HOMO–LUMO (NO → Pb_nAu_n)
CO	−8.951	−1.965				
NO	−11.089	−4.44				
Pb_4Au_4	−4.529	−3.315	2.564	5.636	0.089	7.774
Pb_6Au_6	−4.543	−3.735	2.578	5.216	0.103	7.354
Pb_8Au_8	−4.61	−3.54	2.645	5.411	0.17	7.549

Therefore, Pb_nAu_n clusters are the electron donors and CO molecule is the electron acceptor on the basis of the frontier molecular orbital theory.[53,54] Wang *et al.*[16] also yielded the similar results on HCl molecule adsorption on Au_n–C_2H_2 complexes based on the frontier molecular orbital theory. Moreover, it is also interesting to find that the HOMOs are mainly located on the Au atoms of Pb_nAu_n (n = 4, 6, and 8) clusters and the LUMO is mainly located on the C atom of CO molecule should be responsible for the orientation of C atom of CO molecule directly adsorbed on the Au atoms of Pb_nAu_n (n = 4, 6, and 8) clusters.

The most stable and second stable configurations of NO molecule binding to Pb_nAu_n (n = 4, 6, and 8) clusters were also investigated, as shown in Fig. 3. The initial adsorption configurations of Pb_nAu_n–NO (n = 4, 6, and 8) complexes are similar to that of Pb_nAu_n–CO (n = 4, 6, and 8) complexes. It is found that the NO molecule binds to Pb_nAu_n (n = 4, 6, and 8) clusters by means of N atom (Au–N model), which adopt the similar adsorption configurations with that of NO molecule adsorption onto Ag_7Au_6 clusters.[11,55] The lowest distances between NO molecule and Pb_nAu_n (n = 4, 6, and 8) clusters are in the range of 1.933–1.977 Å, as shown in Table 5, which are larger than the distances between CO molecule and Pb_nAu_n (n = 4, 6, and 8) clusters. The Au–N–O bond angles are in the range of 129.464–135.899°, which shows NO doesn't vertically adsorption onto Pb_nAu_n (n = 4, 6, and 8) clusters. The adsorption energies are in the range of 0.957–1.125 eV, which shows that NO adsorption onto Pb_nAu_n clusters are also chemical processes, as listed in Table 5. The charges are also transferred from the Pb_nAu_n (n = 4, 6, and 8) clusters to NO molecule, which shows the same trend with that of Pb_nAu_n–CO (n = 4, 6, and 8) complexes discussed above. In order to unravel the charges transfer from the Pb_nAu_n (n = 4, 6, and 8) clusters to the NO molecule, we calculated the vibrational frequencies of the –NO moieties in the Pb_nAu_n–NO (n = 4, 6, and 8) complexes, and the vibrational frequency of the isolated NO molecules in the gas phase, as shown in Table 3. From the table, we can see that the vibrational frequencies of the –NO moieties in the Pb_nAu_n–NO (n = 4, 6, and 8) complexes are decreased as compared to the vibrational frequency of the isolated NO molecule in the gas phase. Obviously, the red shifts of the vibrational frequencies of –NO moieties are achieved. It can be used to explain the charges transfer from the Pb_nAu_n clusters to NO molecule in Pb_nAu_n–NO (n = 4, 6, and 8) complexes. In addition, according to the analysis of Pb_nAu_n–CO (n = 4, 6, and 8) complexes, similarly, the HOMOs of Pb_nAu_n (n = 4, 6, and 8) clusters match the LUMO of CO molecule should be responsible for the configurations of Pb_nAu_n–NO complexes and the charges transfer mechanism on the basis of frontier molecular orbital theory. The energy levels of the HOMOs and LUMOs are listed in Table 4, and the diagrams of the HOMOs and LUMOs are shown in Fig. 4.

3.5. The promising applications of Pb_nAu_n (n = 4, 6, and 8) clusters for CO and NO molecules detection

It is well known that the nanoclusters are widely used in nanotechnology, especially in the toxic gas sensing. Herein, we will explore the sensitivity of CO and NO molecule adsorption

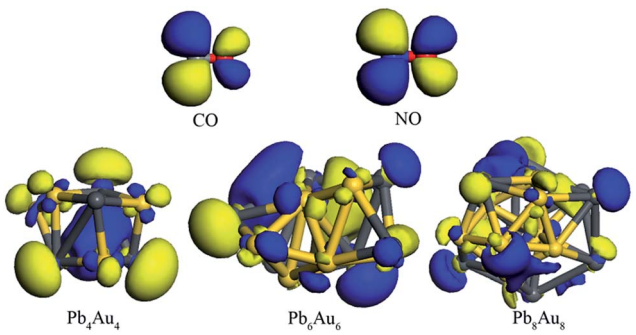

Fig. 4 The HOMOs of Pb_nAu_n (n = 4, 6, and 8) clusters, and LUMOs of CO and NO molecules. The dark gray ball is Pb atom, yellow ball is Au atom, grayish ball is C atom, red ball is O atom, and blue ball is N atom.

Table 5 The calculated adsorption energies (E_{ad}), the distances (D, viewed as the lowest distance between the adsorption site and NO) between NO and Pb_nAu_n (n = 4, 6, and 8) clusters, charges transfer (Q_T) from the Pb_nAu_n clusters to NO (the charges were calculated using Hirshfeld method), HOMO–LUMO gaps (E_g) for the NO adsorption on the Pb_nAu_n (n = 4, 6, and 8) clusters, and ΔE_g represent HOMO–LUMO gap differences between Pb_nAu_n clusters and Pb_nAu_n–NO (n = 4, 6, and 8) complexes ($\Delta E_g = E_g(Pb_nAu_n) - E_g(Pb_nAu_n\text{–NO})$)

Configuration	E_{ads} (eV)	D (Å)	Q_T (e)	E_g (eV)	ΔE_g (eV)
Pb_4Au_4–NO(a)	−1.125	1.943	0.135	0.120	1.094
Pb_4Au_4–NO(b)	−0.995	1.977	0.151	0.270	0.944
Pb_6Au_6–NO(a)	−1.076	1.933	0.132	0.442	0.366
Pb_6Au_6–NO(b)	−1.061	1.948	0.112	0.551	0.257
Pb_8Au_8–NO(a)	−1.152	1.944	0.098	0.611	0.459
Pb_8Au_8–NO(b)	−0.957	1.939	0.134	0.237	0.833

onto Pb_nAu_n (n = 4, 6, and 8) clusters. However, there are two main parameters to judge a nanocluster as an ideal gas sensor:[56] (1) the gas molecules should chemiadsorp onto the nanocluster with a large adsorption energy, because the large adsorption energy can prevent the gas molecule spontaneous desorption from the nanocluster, (2) the gas molecules have a great influence on the electric conductivity of the nanoclusters owing to the sufficient charges transfer between gas molecule and the nanocluster. According to the results and discussion mentioned above, the CO and NO molecules can chemiadsorp onto the Pb_nAu_n clusters (n = 4, 6, and 8), it agrees well with the second condition under which a nanocluster is judged as an ideal gas sensor. Then we will focus on the changes of electric conductivity of the systems before and after the CO or NO molecule adsorption onto the Pb_nAu_n (n = 4, 6, and 8) clusters. The definition of electric conductivity (σ) can be described as the following formula[11,52,57]

$$\sigma \propto \exp\left(\frac{-E_g}{2KT}\right)$$

where E_g, K, and T are the band energy gap of configuration, the Boltzmann's constant, and the thermodynamic temperature, respectively. From the equation, it is find that E_g is responsible for the electric conductivity of the gas molecule before and after adsorption onto the nanocluster. Our results indicating that the HOMO–LUMO gaps of Pb_nAu_n clusters are obviously changed after the CO and NO molecules adsorption onto Pb_nAu_n clusters. The ΔE_g are in the range of 0.157–1.094 eV, as shown in Tables 2 and 5. Hence, the results suggest that the miniaturized sensors based on Pb_nAu_n (n = 4, 6, and 8) clusters can be used to detect the CO and NO molecules by calculating the electric conductivity changes of Pb_nAu_n clusters before and after the molecules adsorption onto the clusters, because the resistance of the system can be easily detected. Moreover, it is possible for CO and NO molecules desorption from the Pb_nAu_n (n = 4, 6, and 8) clusters, which is originated from that Pb_nAu_n clusters are less chemically stable than the Pb_nAu_n–CO and Pb_nAu_n–NO (n = 4, 6, and 8) complexes because the HOMO–LUMO gaps of Pb_nAu_n clusters are larger than that of Pb_nAu_n–CO and Pb_nAu_n–NO complexes. In addition, we will calculate the recovery time τ for gas desorption from Pb_nAu_n (n = 4, 6, and 8) clusters. According the transition state theory, the recovery time τ in terms of adsorption energy E_{ad} can be expressed as[58]

$$\tau = \upsilon_0^{-1} e^{(-E_{ad}/KT)}$$

where T represents the temperature of the system, K stands for the Boltzman's constant (8.62×10^{-5} eV K^{-1}), and υ_0 represents the attempt frequency of the gas molecule ($\upsilon_0 = 10^{12}$ s^{-1} for NO_2 molecules[58]). According to the formula, the recovery time τ increases with the increasing adsorption energy E_{ad}. Here, we assume that the attempt frequencies of CO and NO are equal to that of NO_2. When E_{ad} > 1.0 eV, which corresponds to the recovery time τ > 12 h at room temperature. For the adsorption energies in the range of −0.957 eV to −1.498 eV, the recovery time τ would be in the range of 584 μs to 53 s by means of heating the gas sensors at 550 K.[56] Therefore, the Pb_nAu_n (n = 4, 6 and 8) clusters can be served as reusable gas sensors for CO and NO molecules.

3.6. Density of states

The density of states (DOS) near the fermi levels of the most stable configurations of Pb_nAu_n (n = 4, 6, and 8) clusters, Pb_nAu_n–CO (n = 4, 6, and 8) complexes, and Pb_nAu_n–NO (n = 4, 6, and 8) complexes were carried out, in order to further investigate the increased conductance of Pb_nAu_n–CO (n = 4, 6, and 8) and Pb_nAu_n–NO (n = 4, 6, and 8) complexes, as shown in Fig. 5. The HOMO–LUMO gaps of Pb_nAu_n (n = 4, 6, and 8) clusters are don't obviously reduced when CO molecule is adsorbed on the Pb_nAu_n (n = 4, 6, and 8) clusters, as shown in Table 2. But the

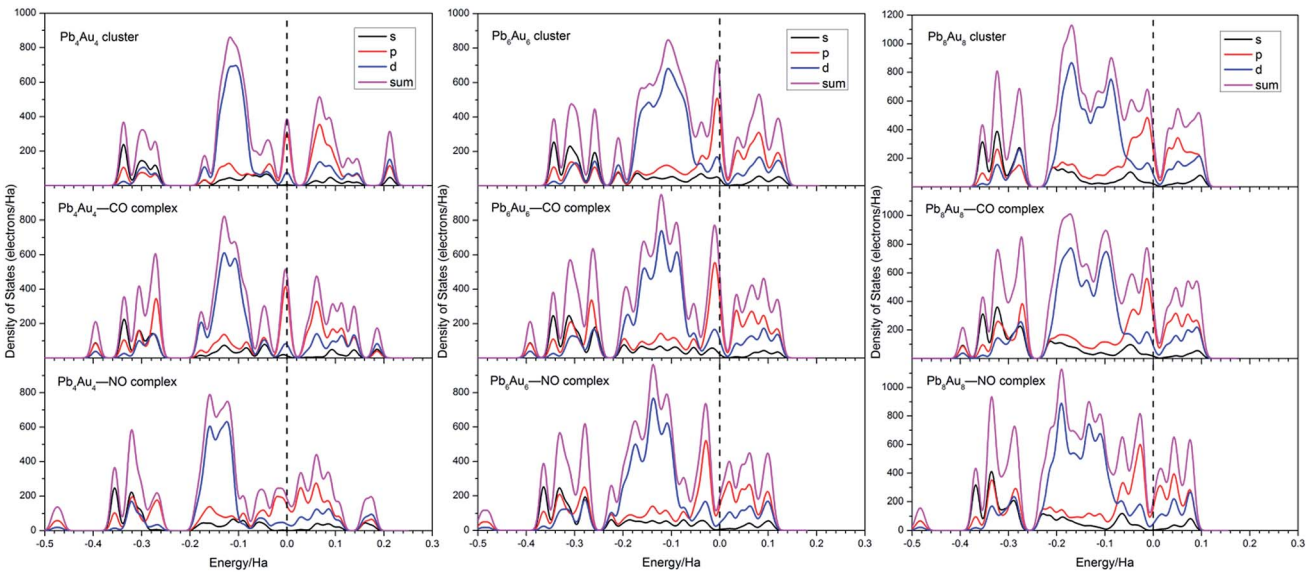

Fig. 5 The density of states (DOS) of the most stable configurations of Pb_nAu_n clusters, Pb_nAu_n–CO complexes, and Pb_nAu_n–NO complexes (n = 4, 6, and 8). The Fermi levels were shifted to zero, and plotted as dashed vertical lines.

HOMO–LUMO gaps of Pb_nAu_n–NO (n = 4, 6, and 8) complexes are obviously reduced compared to that of Pb_nAu_n clusters, as summarized in Table 5. From Fig. 5, the DOS of Pb_nAu_n (n = 4, 6, and 8) clusters do not show distinct changes before and after CO molecule adsorption on the Pb_nAu_n (n = 4, 6, and 8) clusters. It may be attributed to the little charges transfer between the CO molecule and the Pb_nAu_n clusters. However, there are some little changes near the Fermi levels, the DOS above the Fermi levels are slightly shrank and weakly shift toward more negative energy levels. It can be used to explained the decreased HOMO–LUMO gaps of Pb_nAu_n–CO (n = 4, 6, and 8) complexes. According to the Fig. 5, the DOS of Pb_nAu_n–NO (n = 4, 6, and 8) complexes are significantly shift towards to more negative energy levels compared to that of bare Pb_nAu_n (n = 4, 6, and 8) clusters, and the DOS above the Fermi level become more nonlocalized. In other words, the Fermi levels of Pb_nAu_n–NO (n = 4, 6, and 8) complexes shift towards more positive energy levels. Those changes near the Fermi levels should be responsible for the increased conductivities of Pb_nAu_n–NO (n = 4, 6, and 8) complexes.

4. Conclusions

In summary, the ground state structures, average binding energies, fragmentation energies, second order energy differences, HOMO–LUMO gaps, gas sensing, density of states of Pb_nAu_n clusters were systematically investigated on the basis of density functional theory as implemented in DMol^3 package. Based on the structural growth pattern of the ground state structures of Pb_nAu_n (n = 2–12) clusters, the Au atoms tend to aggregate together and occupy the geometrical centers of Pb_nAu_n clusters. The average binding energies show a generally increasing tendency to be stable at the beginning of cluster size n = 10. The fragmentation energies and second order energy differences show obvious odd–even alternations, indicating that the Pb_nAu_n clusters with close shell electrons are more stable than their neighboring clusters with open shell electrons. Pb_4Au_4, Pb_6Au_6 and Pb_8Au_8 clusters are the magic clusters with chemically stable reactivity. Moreover, Pb_nAu_n (n = 4, 6, and 8) have great potential in CO and NO molecules detection. The gas sensing properties of Pb_nAu_n clusters will be further verified by experimental results.

Conflicts of interest

There are no conflicts of interest to declare.

Acknowledgements

This work was financially supported by the Regional Foundation of the NSFC (51664032), the Foundation of the State Key Laboratory of Complex Nonferrous Metal Resources Clear Utilization (CNMRCUTS1503), the Joint Foundation of the NSFC-Yunnan province (U1502271), the Leader in Science and Technology of Yunnan Province (2014HA003), the Program for Nonferrous Metals Vacuum Metallurgy Innovation Team of Ministry of Science and Technology (2014RA4018), the National Key Research and Development Program of China (2016YFC0400404) and the Program for Innovative Research Team in University of Ministry of Education of China (No. IRT_17R48).

References

1 I. M. L. Billas, A. Châtelain and W. A. de Heer, *Science*, 1994, **265**, 1682.
2 H. Yang, Y. Wang, X. Chen, X. Zhao, L. Gu, H. Huang, J. Yan, C. Xu, G. Li, J. Wu, A. J. Edwards, B. Dittrich, Z. Tang, D. Wang, L. Lehtovaara, H. Häkkinen and N. Zheng, Plasmonic twinned silver nanoparticles with molecular precision, *Nat. Commun.*, 2016, **7**, 12809.
3 T. Zhou, J. J. Goings and Z. Lin, *J. Phys. Chem. A*, 2016, **120**, 8485.
4 P.-C. Chen, Y.-C. Li, J.-Y. Ma, J.-Y. Huang, C.-F. Chen and H.-T. Chang, *Sci. Rep.*, 2016, **6**, 24882.
5 A. P. Alivisatos, *Science*, 1996, **271**, 933.
6 M. C. Daniel and D. Astruc, *Chem. Rev.*, 2004, **104**, 293.
7 Q. Y. Lin, Z. Li, K. A. Brown, M. N. O'Brien, M. B. Ross, Y. Zhou, S. Butun, P. C. Chen, G. C. Schatz and V. P. Dravid, *Nano Lett.*, 2015, **15**, 4699.
8 Y.-R. Zhao, X.-Y. Kuang, B.-B. Zheng, Y.-F. Li and S.-J. Wang, *J. Phys. Chem. A*, 2011, **115**, 569.
9 C. L. Cleveland, U. Landman, T. G. Schaaff, M. N. Shafigullin, P. W. Stephens and R. L. Whetten, *Phys. Rev. Lett.*, 1997, **79**, 1873.
10 S. H. Yau, O. Varnavski and T. Goodson, *Acc. Chem. Res.*, 2013, **46**, 1506.
11 Y. Yong, C. Li, X. Li, T. Li, H. Cui and S. Lv, *J. Phys. Chem. C*, 2015, **119**, 7534.
12 K. Mondal, A. Banerjee and T. K. Ghanty, *J. Phys. Chem. C*, 2014, **118**, 11935.
13 Y. Chen, H. Wang, C.-J. Liu, Z. Zeng, H. Zhang, C. Zhou, X. Jia and Y. Yang, *J. Catal.*, 2012, **289**, 105.
14 Z. Y. Li, N. P. Young, M. Di Vece, S. Palomba, R. E. Palmer, A. L. Bleloch, B. C. Curley, R. L. Johnston, J. Jiang and J. Yuan, *Nature*, 2008, **451**, 46.
15 D. R. Kauffman, D. Alfonso, C. Matranga, H. Qian and R. Jin, *J. Am. Chem. Soc.*, 2012, **134**, 10237.
16 Y. Wang, M. Zhu, L. Kang and B. Dai, *RSC Adv.*, 2014, **4**, 38466.
17 H. S. De, S. Krishnamurty, D. Mishra and S. Pal, *J. Phys. Chem. C*, 2011, **115**, 17278.
18 S. Gautam and A. D. Sarkar, *Phys. Chem. Chem. Phys.*, 2016, **18**, 13830.
19 X. B. Li, H. Y. Wang, X. D. Yang, Z. H. Zhu and Y. J. Tang, *J. Chem. Phys.*, 2007, **126**, 084505.
20 B. Assadollahzadeh and P. Schwerdtfeger, *J. Chem. Phys.*, 2009, **131**, 064306.
21 H. Haekkinen, B. Yoon, U. Landman, X. Li, H. J. Zhai and L. S. Wang, *J. Phys. Chem. A*, 2003, **107**, 6168.
22 B. Assadollahzadeh and P. Schwerdtfeger, *J. Chem. Phys.*, 2009, **131**, 064306.
23 H. Häkkinen, M. Moseler and U. Landman, *Phys. Rev. Lett.*, 2002, **89**, 033401.

24 X. Gu, M. Ji, S. H. Wei and X. G. Gong, *Phys. Rev. B: Condens. Matter Mater. Phys.*, 2004, **70**, 205401.
25 B. S. de Bas, M. J. Ford and M. B. Cortie, *J. Mol. Struct.: THEOCHEM*, 2004, **686**, 193.
26 M. Zhou, C. Zeng, Y. Chen, S. Zhao, M. Y. Sfeir, M. Zhu and R. Jin, *Nat. Commun.*, 2016, **7**, 13240.
27 X. Li, B. Kiran, L.-F. Cui and L.-S. Wang, *Phys. Rev. Lett.*, 2005, **95**, 253401.
28 H. Wen, Y. R. Liu, T. Huang, K. M. Xu, W. J. Zhang, W. Huang and L. S. Wang, *J. Chem. Phys.*, 2013, **138**, 174303.
29 H. Wen, Y.-R. Liu, K.-M. Xu, T. Huang, C.-J. Hu, W.-J. Zhang and W. Huang, *RSC Adv.*, 2014, **4**, 15066.
30 Y. R. Liu, T. Huang, Y. B. Gai, Y. Zhang, Y. J. Feng and W. Huang, *Sci. Rep.*, 2015, **5**, 17738.
31 D. R. Kauffman, D. Alfonso, C. Matranga, H. Qian and R. Jin, *J. Phys. Chem. C*, 2013, **117**, 7914.
32 M. Zhang, L.-M. He, L.-X. Zhao, X.-J. Feng and Y.-H. Luo, *J. Phys. Chem. C*, 2009, **113**, 6491.
33 M. Zhang, H. Zhang, L. Zhao, Y. Li and Y. Luo, *J. Phys. Chem. A*, 2012, **116**, 1493.
34 G. Mills, M. S. Gordon and H. Metiu, *Chem. Phys. Lett.*, 2002, **359**, 493.
35 W. Zhang, D. Cheng and J. Zhu, *RSC Adv.*, 2014, **4**, 42554.
36 G. Li, J. Wang, X. Chen, Z. Zhou, H. Yang, B. Yang, B. Xu and D. Liu, *Comput. Theor. Chem.*, 2017, **1106**, 21.
37 S. Nosé, *Mol. Phys.*, 2002, **52**, 255.
38 B. Wang, J. Zhao, X. Chen, D. Shi and G. Wang, *Phys. Rev. A*, 2005, **71**, 033201.
39 M. Hu, D. P. Linder, M. B. Nardelli and A. Striolo, *J. Phys. Chem. C*, 2013, **117**, 15050.
40 C. Rajesh and C. Majumder, *J. Chem. Phys.*, 2008, **128**, 024308.
41 H. Xie, Z. Qin, X. Wu, Z. Tang and L. Jiang, *J. Chem. Phys.*, 2012, **137**, 064318.
42 M. E. Eberhart, R. C. O'Handley and K. H. Johnson, *Phys. Rev. B: Condens. Matter Mater. Phys.*, 1984, **29**, 1097.
43 C. Rajesh and C. Majumder, *J. Chem. Phys.*, 2007, **126**, 244704.
44 J.-Q. Wen, J.-M. Zhang, G.-X. Chen, X.-Z. Zhang and Z.-Y. Wen, *J. Phys. Chem. Solids*, 2016, **96–97**, 68.
45 R. Trivedi and D. Bandyopadhyay, *Int. J. Hydrogen Energy*, 2016, **41**, 20113.
46 L. R. Radovic and B. Bockrath, *J. Am. Chem. Soc.*, 2005, **127**, 5917.
47 Z. Mahdavifar and M. Haghbayan, *Appl. Surf. Sci.*, 2012, **263**, 553.
48 W. D. Knight, K. Clemenger, W. A. de Heer, W. A. Saunders, M. Y. Chou and M. L. Cohen, *Phys. Rev. Lett.*, 1984, **52**, 2141.
49 M. L. Cohen, M. Y. Chou, W. D. Knight and W. A. De Heer, *J. Phys. Chem.*, 1987, **91**, 3141.
50 X. Huang, Y. Su, L. Sai, J. Zhao and V. Kumar, *J. Cluster Sci.*, 2015, **26**, 389.
51 K. Mondal, D. Manna, T. K. Ghanty and A. Banerjee, *Chem. Phys.*, 2014, **428**, 75.
52 Y. Yong, H. Jiang, X. Li, S. Lv and J. Cao, *Phys. Chem. Chem. Phys.*, 2016, **18**, 21431.
53 K. N. Houk, *Acc. Chem. Res.*, 1975, **8**, 361.
54 K. Fukui, *Recognition of Stereochemical Paths by Orbital Interaction*, 1971, pp. 244–251.
55 R. Q. Wu, M. Yang, Y. H. Lu, Y. P. Feng, Z. G. Huang and Q. Y. Wu, *J. Phys. Chem. C*, 2015, **112**, 15985.
56 J. Kong, N. R. Franklin, C. Zhou, M. G. Chapline, S. Peng, K. Cho and H. Dai, *Science*, 2000, **287**, 622.
57 A. Ahmadi, N. L. Hadipour, M. Kamfiroozi and Z. Bagheri, *Sens. Actuators, B*, 2012, **161**, 1025.
58 S. Peng, K. Cho, P. Qi and H. Dai, *Chem. Phys. Lett.*, 2004, **387**, 271.